Available online at www.sciencedirect.com

SciVerse ScienceDirect

Ceramics International 38 (2012) 5123–5131

CERAMICS INTERNATIONAL

www.elsevier.com/locate/ceramint

Characterization of $Ba_{0.5}Sr_{0.5}M_{1-x}Fe_xO_{3-\delta}$ (M = Co and Cu) perovskite oxide cathode materials for intermediate temperature solid oxide fuel cells

Ki-Woog Song [a], Ki-Tae Lee [a,b,*]

[a] Division of Advanced Materials Engineering, Chonbuk National University, Jeonbuk 560-756, Republic of Korea
[b] Hydrogen and Fuel Cells Research Center, Chonbuk National University, Jeonbuk 560-756, Republic of Korea

Received 5 August 2011; received in revised form 5 March 2012; accepted 6 March 2012
Available online 14 March 2012

Abstract

$Ba_{0.5}Sr_{0.5}Co_{1-x}Fe_xO_{3-\delta}$ ($x = 0.2$, 0.6, and 0.8) and $Ba_{0.5}Sr_{0.5}Cu_{1-x}Fe_xO_{3-\delta}$ ($x = 0.6$ and 0.8) perovskite oxides have been investigated as cathode materials for intermediate temperature solid oxide fuel cells. All the samples synthesized by a citrate–EDTA complexing method were single-phase cubic perovskite solid solutions. Then, the thermal expansion coefficient, electrical conductivities, the oxygen vacancy concentrations, the polarization resistances (R_p), and the power densities were measured. An increase in the Co content resulted in a decrease in the polarization resistance, the electrical conductivities at low temperatures, and the inflection point of the thermal expansion coefficient, but it led to an increase in the electrical conductivities at high temperatures, the oxygen vacancy concentrations, and the maximum power densities. The Cu-based system has similar behavior to the Co-based system; yet, in terms of the electrical conductivities, high Cu content gave a better result than low content for the entire range of temperatures.

Keywords: C. Electrical conductivity; C. Thermal expansion; D. Perovskite; Solid oxide fuel cells

1. Introduction

Solid oxide fuel cells (SOFCs) have high energy conversion efficiency, low pollution emissions, and other environmental advantages that make them an attractive alternative to other energy conversion devices. Recently, intermediate temperature SOFCs (IT-SOFCs), which operate in the range of 500–800 °C, have drawn attention due to their versatility in terms of components, mechanical stability, decreased chemical reactivity, and other favorable attributes. Unfortunately, conventional cathode materials such as $La_{1-x}Sr_xMnO_3$ do not have enough catalytic activity to induce the oxygen reduction reaction in the intermediate temperature range due to their low oxygen ion vacancy concentrations, which result in low oxygen permeability and thereby limit the oxygen reduction rates in the triple-phase boundary (TPB) [1,2]. Consequently, discovering alternative candidates for IT-SOFC cathodes has become a high research priority.

Mixed-conduction perovskite oxides have been extensively explored as cathode materials for IT-SOFCs because they possess an ideal combination of electronic and ionic conductivities, a beneficial electrochemical reaction, and a fine structural stability [3–8]. In particular, $La_{0.6}Sr_{0.4}Co_{0.2}Fe_{0.8}O_{3-\delta}$ (LSCF) has been reported to perform exceptionally well as an IT-SOFC cathode material [9–13].

Since Shao et al. first discovered $Ba_{0.5}Sr_{0.5}Co_{0.8}Fe_{0.2}O_{3-\delta}$ (BSCF), which substitutes Ba, a divalent alkaline-earth element, for La, a trivalent rare-earth element, in the $La_{1-x}Sr_xCo_{1-y}Fe_yO_{3-\delta}$ composition, and BSCF and modified-BSCF have been widely studied as promising cathode materials in IT-SOFCs [6–8,14–16]. BSCF is a prospective cathode material because it has a high catalytic activity for the oxygen reduction reaction and a good oxygen diffusion rate [6–8,14]; however, BSCFs with a high Co content also have a large thermal expansion coefficient (TEC), which can cause considerable problems, such as decreased mechanical stability with the other cell components [17–19].

* Corresponding author at: Division of Advanced Materials Engineering, Chonbuk National University, Jeonbuk 560-756, Republic of Korea.
Tel.: +82 63 270 2290; fax: +82 63 270 2386.
E-mail address: ktlee71@jbnu.ac.kr (K.-T. Lee).

0272-8842/$36.00
doi:10.1016/j.ceramint.2012.03.015

Thus, the objective of this study was to improve the electrical conductivity and reduce the TEC of BSCF by substituting various amounts of Co and Cu onto the B site of BSCF, all while retaining its remarkable electrochemical reaction. To do so, $Ba_{0.5}Sr_{0.5}Co_{1-x}Fe_xO_{3-\delta}$ ($x = 0.2$, 0.6, and 0.8; BSCoF) and $Ba_{0.5}Sr_{0.5}Cu_{1-x}Fe_xO_{3-\delta}$ ($x = 0.6$ and 0.8; BSCuF) were synthesized using a citrate–EDTA complexing method, and the effects of Co and Cu on the oxide ion vacancy concentrations, the TECs, the electrical conductivities, and the electrochemical performances were investigated. In addition, all the compositions were compared to LSCF to determine their relative performances.

2. Experimental procedure

All cathode powders were synthesized using a citrate-EDTA complexing method [20]. The nomenclature for each composition is listed in Table 1. The required amount of ethylenediamine-tetraacetic acid (EDTA) was initially dissolved in aqueous NH_4OH. The stoichiometric quantity of metal nitrates, $Ba(NO_3)_2$, $Sr(NO_3)_2$, $Co(NO_3)_2{\cdot}6H_2O$, $Cu(NO_3)_2{\cdot}2.5H_2O$, $Fe(NO_3)_3{\cdot}9H_2O$, and $La(NO_3)_3{\cdot}6H_2O$, for each composition was then added to the EDTA–NH_4OH solution under stirring. Next, an appropriate amount of citric acid was mixed with the solution, and NH_4OH was added until the pH reached ~8. The molar ratio of the EDTA/citric acid/metal ions was 1:1.5:1. The precursor was kept at 90 °C with stirring to evaporate the water. After transparent gels were obtained, they were dried in an oven at 130 °C for 24 h, creating porous ashes. These ashes were then calcined at 900 °C for 5 h in air to obtain end-products possessing a single phase of the perovskite structure. The $Ce_{0.8}Gd_{0.2}O_{1.9}$ (GDC) electrolyte was prepared by the urea combustion method [21]. The dense GDC electrolyte was sintered at 1450 °C for 4 h, and the anode powder (Ni:YSZ = 60:40 vol%) was prepared by ball milling for 12 h with NiO (FP, Japan) and 8YSZ (Tosoh, Japan) commercial powders.

The phase identification of the prepared powders was carried out using an X-ray diffractometer (XRD, D/MAX-111A, Rigaku Corporation, Japan) with a scanning speed of 4°/min using Cu Kα radiation. Microstructural characterization of the prepared samples was carried out with a scanning electron microscope (SEM, SN-3000 Hitachi, Japan). Iodometric titration was performed at room temperature in order to investigate the oxygen vacancy concentration, δ, for all the cathode compositions except LSCF. The variation of oxygen contents with temperature (25–900 °C) was assessed with a Perkin-Elmer Series 7 thermogravimetric analyzer (TGA) in air with a heating/cooling rate of 2 °C/min. In order to exclude moisture effect, all samples were heated at 200 °C for 6 h before TGA experiment. The electrical conductivities were measured via a four-probe DC method in the range of 300-800 °C at 50 °C increments in air and oxygen atmosphere, respectively. Thermal expansion coefficients (TECs) were observed using TMA from room temperature to 800 °C with a heating/cooling rate of 2 °C/min in air. For the electrical conductivity and TEC measurements, the BSCoF, BSCuF, and LSCF samples were sintered at 1100, 900, and 1200 °C for 5, 10, and 5 h, respectively. All the samples used for conductivity and TEC measurements had densities greater than 95% of the theoretical values.

Electrochemical performances were evaluated via AC impedance analysis and current–voltage (I–V) measurements with electrolyte-supported symmetrical half cells and single cells, respectively. The screen printed cathodes were fired at 925 °C (BSCuF) and 1000 °C (BSCoF and LSCF) for 2 h. The symmetrical half cells with a geometrical electrode area of

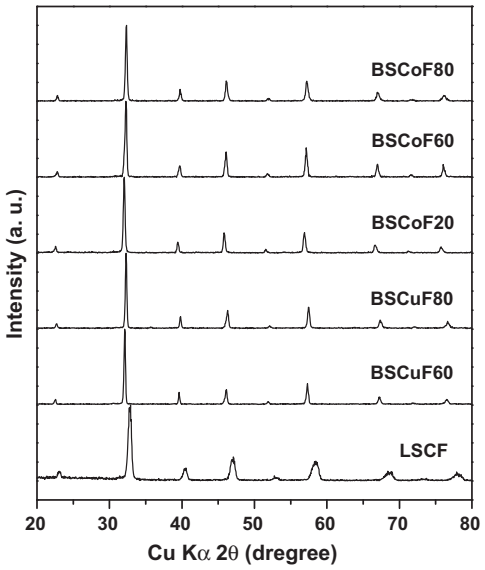

Fig. 1. X-ray diffraction patterns of $Ba_{0.5}Sr_{0.5}Co_{1-x}Fe_xO_{3-\delta}$ ($x = 0.2$, 0.6, and 0.8), $Ba_{0.5}Sr_{0.5}Cu_{1-x}Fe_xO_{3-\delta}$ ($x = 0.6$ and 0.8), and $La_{0.6}Sr_{0.4}Co_{0.2}Fe_{0.8}O_{3-\delta}$ (LSCF) oxides calcined at 900 °C for 5 h.

Table 1
Nomenclature for the synthesized powders.

Composition	Abbreviation
$Ba_{0.5}Sr_{0.5}Co_{0.8}Fe_{0.2}O_{3-\delta}$	BSCoF20
$Ba_{0.5}Sr_{0.5}Co_{0.4}Fe_{0.6}O_{3-\delta}$	BSCoF60
$Ba_{0.5}Sr_{0.5}Co_{0.2}Fe_{0.8}O_{3-\delta}$	BSCoF80
$Ba_{0.5}Sr_{0.5}Cu_{0.4}Fe_{0.6}O_{3-\delta}$	BSCuF60
$Ba_{0.5}Sr_{0.5}Cu_{0.2}Fe_{0.8}O_{3-\delta}$	BSCuF80
$La_{0.6}Sr_{0.4}Co_{0.2}Fe_{0.8}O_{3-\delta}$	LSCF

Table 2
B-site mean valence and oxygen content ($3 - \delta$) data as measured by iodometric titration at room temperature.

Composition	Mean valence of B-site cations	Oxygen content ($3 - \delta$)
BSCoF20	3.24	2.62
BSCoF60	3.27	2.64
BSCoF80	3.33	2.67
BSCuF60	2.90	2.45
BSCuF80	2.98	2.49
LSCF	3.35 [26]	2.97 [26]

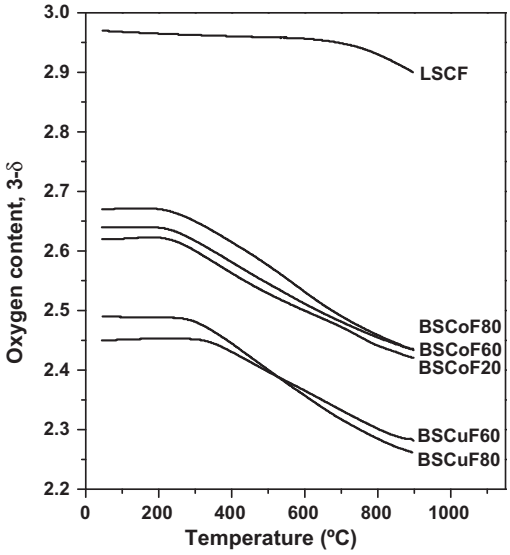

Fig. 2. The oxygen content $(3-\delta)$ as a function of temperature in $Ba_{0.5}Sr_{0.5}Co_{1-x}Fe_xO_{3-\delta}$ ($x = 0.2$, 0.6, and 0.8), $Ba_{0.5}Sr_{0.5}Cu_{1-x}Fe_xO_{3-\delta}$ ($x = 0.6$ and 0.8), and $La_{0.6}Sr_{0.4}Co_{0.2}Fe_{0.8}O_{3-\delta}$ (LSCF) oxides determined from iodometric titration (room temperature) and TGA from room temperature to 900 °C.

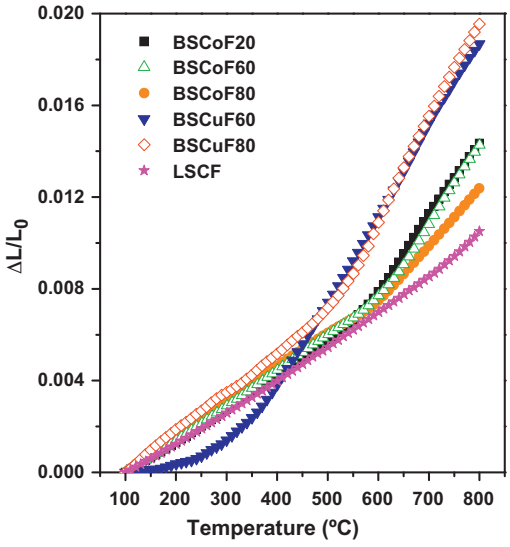

Fig. 3. Thermal expansion behaviors of BSCoF, BSCuF, and LSCF samples sintered at 1100, 900, and 1200 °C for 5, 10, and 5 h, respectively, in the temperature range of 100–800 °C.

0.25 cm^2 were monitored by AC impedance spectroscopy with an applied frequency range of 1 mHz–100 kHz and with a voltage amplitude of 20 mV. Current–voltage (*I–V*) measurements of the single cells with three electrodes, which allowed for the separation and monitoring of the cathode over-potentials during the cell operation, were carried out at 800 °C using a cathode/GDC electrolyte/Ni-8YSZ cermet anode. Pt paste was used as the reference electrode on the cathode side. The cathodes and the Ni-8YSZ cermet anode were prepared by screen printing onto a 0.8-mm-thick GDC electrolyte pellet, followed by firing for 2 h at 925–1000 °C for the cathode and 1200 °C for the anode. The geometrical area of the electrode was 0.25 cm^2. Humidified H_2 (~3% H_2O at 30 °C) and dry air were supplied at a rate of 60 cm^3/min as fuel and oxidant to the anode and cathode, respectively.

3. Results and discussion

3.1. Crystal chemistry and defect structure

The X-ray diffraction patterns of the $Ba_{0.5}Sr_{0.5}Co_{1-x}Fe_xO_{3-\delta}$ ($x = 0.2$, 0.6, and 0.8), $Ba_{0.5}Sr_{0.5}Cu_{1-x}Fe_xO_{3-\delta}$ ($x = 0.6$ and 0.8),

Table 3
Linear TECs of BSCoF, BSCuF, and LSCF samples calculated from the thermal expansion curves with temperature.

Sample	TEC ($\times 10^{-6}$/°C)		
	Low temperature region	High temperature region	Overall
BSCoF20	15.2	34.2	19.6
BSCoF60	14.8	32.4	19.0
BSCoF80	14.7	24.4	16.5
BSCuF60	7.6	37.2	29.2
BSCuF80	17.4	44.4	27.1
LSCF	14.3	20.2	14.7

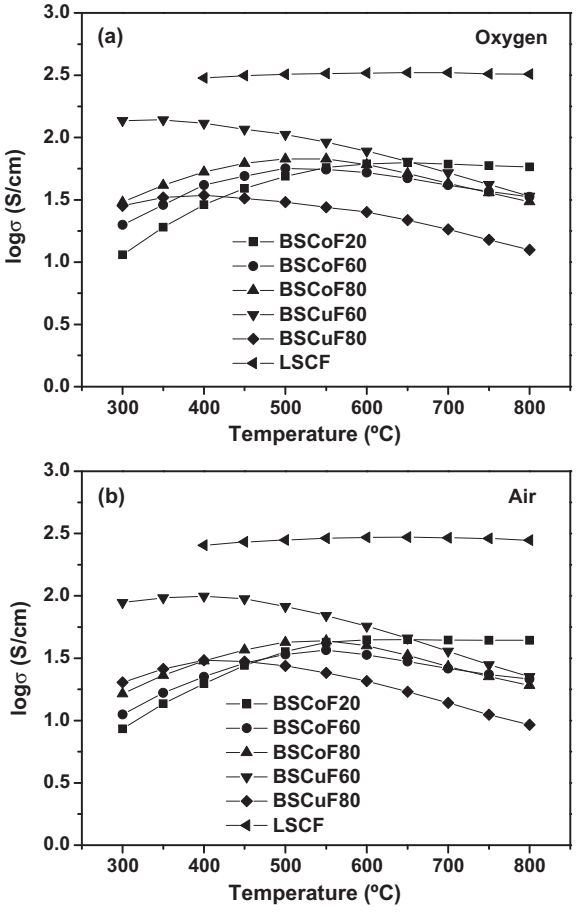

Fig. 4. Variation in the electrical conductivity of BSCoF, BSCuF, and LSCF oxides measured in (a) oxygen and (b) air atmospheres.

and $La_{0.6}Sr_{0.4}Co_{0.2}Fe_{0.8}O_{3-\delta}$ (LSCF) samples synthesized by the citrate–EDTA complexing method and calcined at 900 °C for 5 h are shown in Fig. 1. All patterns show a typical perovskite structure without any impurities. While BSCoF and BSCuF were found to be cubic structures, LSCF was found to be a rhombohedral structure.

The average oxidation state values for the transition metal ions on the B-site of the perovskite structure and the oxygen content determined by iodometric titration at room temperature are summarized in Table 2. The variations of the oxygen content with temperature in the samples are also shown in Fig. 2. The oxygen stoichiometries measured in this work lies within the range reported in the literature [22]. Note that the oxygen nonstoichiometry increases with increasing Co and Cu content. Since Ba and Sr have a fixed valence state of +2 in the BSCoF and BSCuF perovskite, B-site elements such as

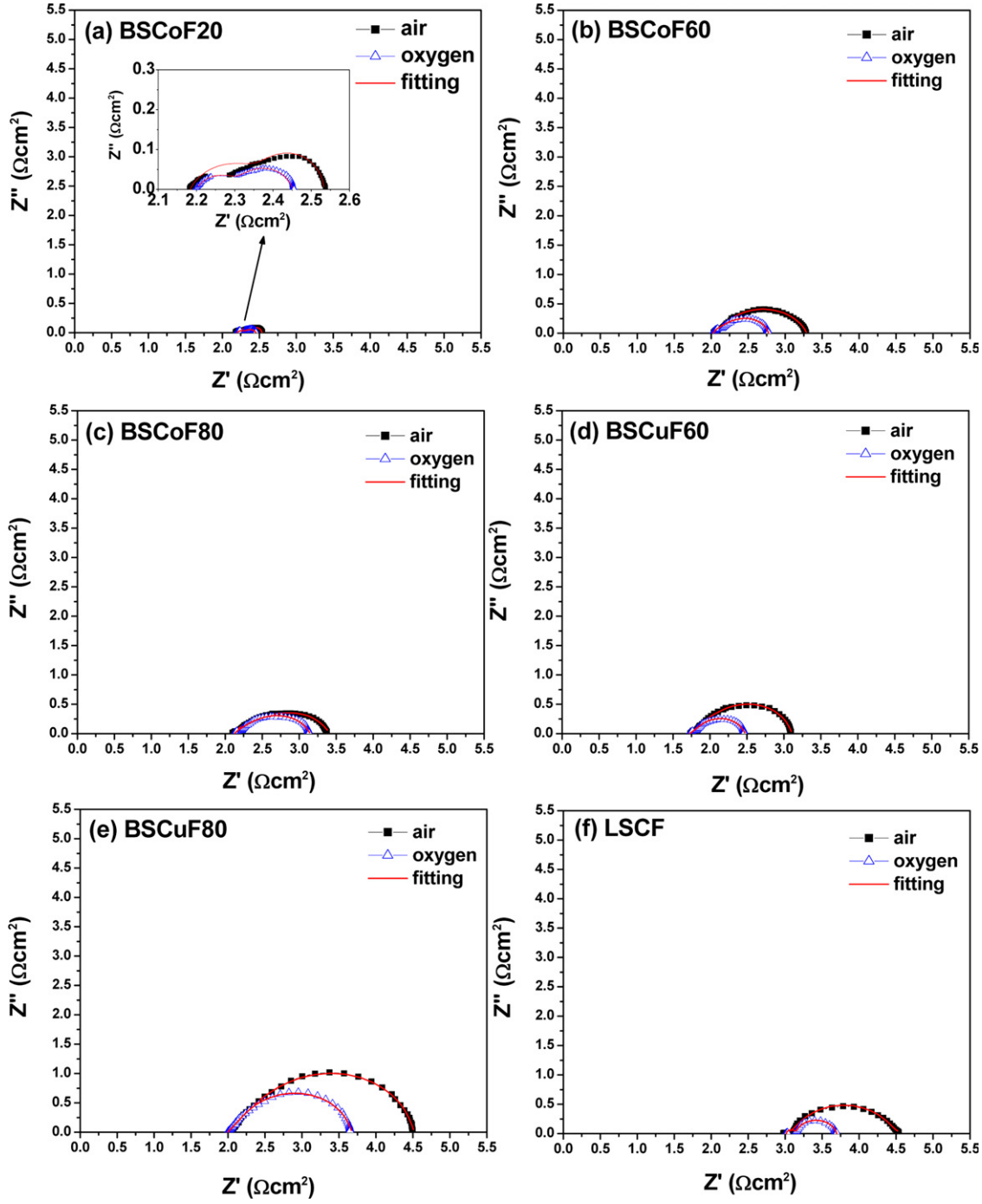

Fig. 5. Typical AC impedance spectra of the symmetrical half cells with the various cathodes on the GDC electrolyte in air or oxygen atmospheres at 600 °C: (a) BSCoF20, (b) BSCoF60, (c) BSCoF80, (d) BSCuF60, (e) BSCuF80, and (f) LSCF.

Co, Cu, and Fe need to take +4 valence states to be electrically neutralized. However, it is difficult to change Co from a trivalent state to a tetravalent state in the B-site of perovskite, so a considerable amount of Co might remain as Co^{3+} ions. Fe ions, on the other hand, easily form a tetravalent state [23]. Cu does not exist well in a +4 valence state in air, so all the Cu would remain as Cu^{2+} or Cu^{3+} [24,25]. As a result, both Co and Cu lead to a large amount of oxide ion vacancies. In particular, the Cu-doped compositions introduce remarkable oxygen nonstoichiometry. In contrast to BSCoF and BSCuF, since La and Sr in the A-site of LSCF perovskite are fixed valence ions, likewise, La^{3+} and Sr^{2+}, the mean valence state of Co and Fe in B-site is much lower than +4 valence state at +3.4, and 0.8 mol of Fe ions easily form a tetravalent state might be enough to make charge compensation in LSCF [23,26]. Therefore, LSCF creates a smaller number of oxygen vacancies compared to BSCoF and BSCuF.

3.2. Thermal expansion behavior

The thermal expansion behaviors of the BSCoF, BSCuF, and LSCF samples sintered at 1100, 900, and 1200 °C for 5, 10, and 5 h, respectively, in the temperature range of 100–800 °C, are presented in Fig. 3, and the calculated TEC values for the different temperature ranges are listed in Table 3. It has been reported that the introduction of Co in the B-site of a perovskite structure causes an increase in the TEC [26–28]. In the BSCoF samples, the average TEC increased with increasing Co content, as shown in Fig. 3 and Table 3. This TEC increase can be attributed to the higher degree of oxide ion vacancies and the low-spin to high-spin transition associated with the Co^{3+} ion [29–31]. For instance, a significant quantity of Co^{3+} ions is present in BSCoF [23], and the number of Co^{3+} ions increases with increasing Co content. Additionally, the Co^{3+} ions experience a spin transition from the smaller ionic radius of the low spin Co^{3+} ion ($r = 0.545$ Å) to the higher radius of the high spin Co^{3+} ion ($r = 0.61$ Å) with increasing temperature [29,30], which leads to an increase in the TEC [32]. Moreover, oxide ion vacancies induce a reduction in the electrostatic bond strength, which is inversely proportional to the TEC [31]. Thus, it can be concluded that an increase in the TEC with increasing Co content in the BSCoF samples is also due to an increase in the concentration of oxide ion vacancies. At the same time, the inflection point of the TEC was observed to have also risen slightly with the increasing Co content. This result, which demonstrates the effects of the formation of oxide ion vacancies on the TEC, corresponds to oxygen non-stoichiometry results found in Table 2 and Fig. 2.

In a Cu-doped system, it has been reported that the substitution of Co with Cu in the LSCF system decreases the TEC due to the significant overlap of orbitals with a covalent character [33]. However, the BSCuF oxides exhibits a much larger average TEC compared with the BSCoF oxides. This phenomenon can be explained by the presence of a considerable number of oxide ion vacancies. As shown in Table 2 and Fig. 2, BSCuF possesses much larger quantities of oxide ion deficiencies than BSCoF because of the Cu ions, which supports the above explanation. Accordingly, a markedly elevated TEC was observed in the BSCuF sample, and the TEC increased with increasing Cu content. In comparison, LSCF showed lower TEC values than did BSCoF and BSCuF, most likely because it possesses fewer oxide ion vacancies.

3.3. Electrical conductivity

Fig. 4 shows the electrical conductivities of BSCoF, BSCuF, and LSCF measured in oxygen and air atmosphere, respectively, as a function of temperature. The electrical conductivities of all of the compositions were found to increase to a maximum with increasing temperature, and then decrease with a further increase in the operation temperature in oxygen and air. A decrease in the conductivity at high temperatures could explain the oxygen loss from the lattice, since the formation of oxide ion vacancies tends to

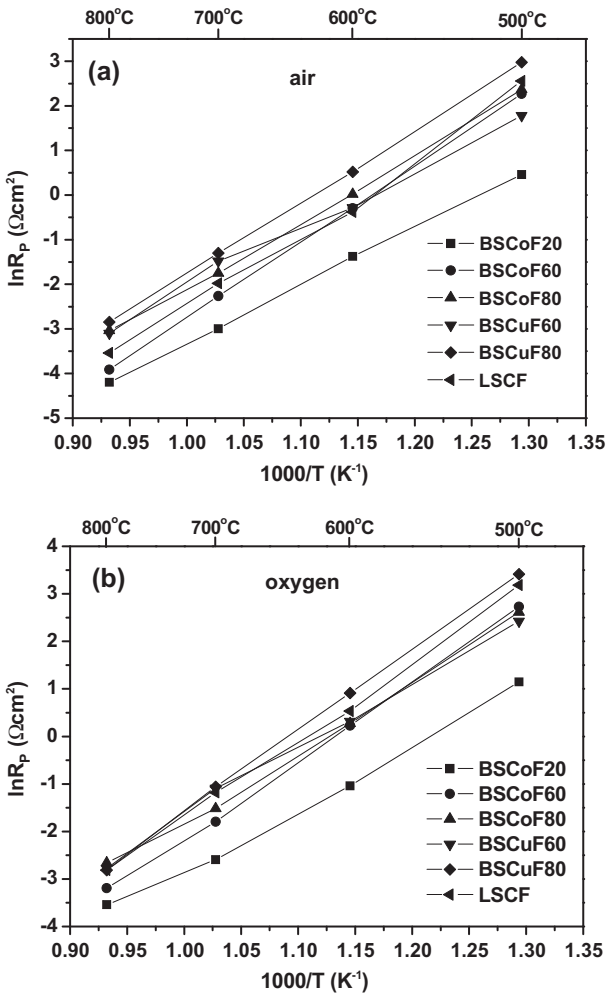

Fig. 6. Temperature dependence of the polarization resistance (R_P) in (a) air and (b) oxygen with the cathodes/GDC/cathodes symmetrical half cell as derived from the AC impedance data.

decrease the carrier mobility and (Co/Cu,Fe)–O–(Co/Cu,Fe) periodic potential [34]. In particular, for BSCuF, the magnitude of the observed conductivity value increased with increasing Cu content, and the conductivity of BSCuF, especially BSCuF60, exhibited better values than those of BSCoF at low temperatures because of the Cu valence state in the B^{4+} site in the BSCuF perovskite. As explained above, Cu exists in divalent and trivalent states, which creates charge carriers. Therefore, BSCuF had relatively higher electrical conductivity with a highly effective charge carrier, $B_{Cu^{2+}}$, in the low temperature range. However, lower conductivity values for BSCuF were observed with a subsequent increase to higher temperatures when compared to BSCoF. This observation may be closely related to the release of lattice oxygen from the oxides. BSCuF possesses a greater number of oxygen vacancies, as shown in Table 2 and Fig. 2, which may increase dramatically with the thermal reduction of Cu^{3+}/Fe^{4+} to Cu^{2+}/Fe^{3+} and with an increase in temperature to carry out the charge compensation. As a result, significant quantities of oxide ion vacancies would be generated at high temperatures. The phenomenon of the low conductivity of BSCuF versus BSCoF in the high temperature region can therefore be attributed to the decline in carrier mobility and (Cu,Fe)–O–(Cu,Fe) periodic potential. In the BSCoF samples, as Co content increased, the electrical conductivity decreased in the low temperature region because the number of oxide ion vacancies increased. After reaching a maximum, the conductivity values diminished more steadily with Co quantity, which consequently led to an increase in the total conductivity relative to the Co magnitude in the high temperature region. This change might have been caused by the generation of charge carriers from thermally reduced Co ions, Co^{4+} to Co^{3+}. From the viewpoint of bond strength, the Fe–O bond is stronger than the Co–O bond [35], thus the thermal reduction of Co ions should be easier than that of Fe ions. Hence, with increasing

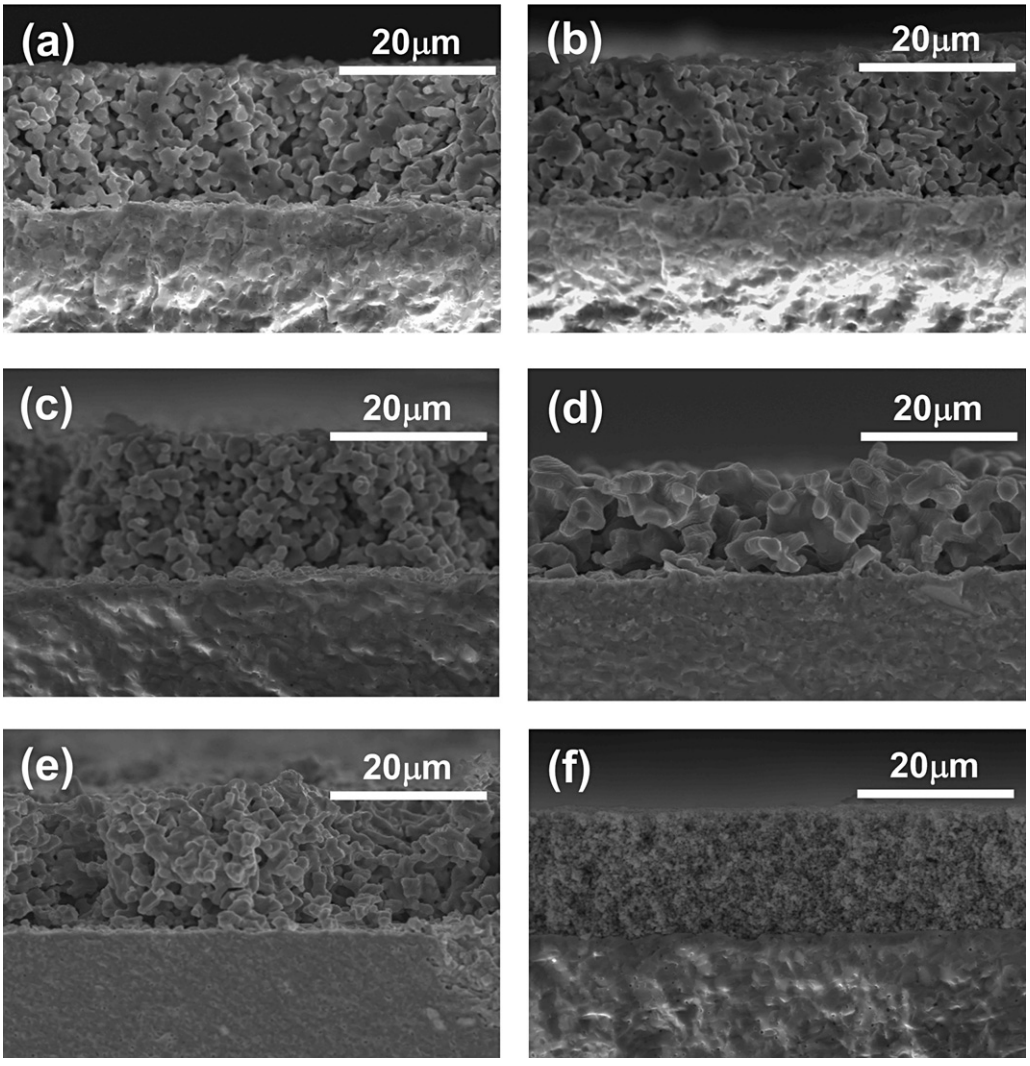

Fig. 7. SEM micrographs of (a) BSCoF20, (b) BSCoF60, (c) BSCoF80, (d) BSCuF60, (e) BSCuF80, and (f) LSCF cathodes on the GDC electrolyte after a single cell test at 800 °C.

Co content, more charge carriers such as $Co^{3+\prime}_{B4+}$ might be generated, which could explain the superior conductivity values and steady electrical conductivity reduction that was observed in the high temperature region.

3.4. Electrochemical performance

The typical AC impedance spectra of the symmetrical half cells with the GDC electrolyte and the cathodes at 600 °C in oxygen and air atmosphere, respectively, are shown in Fig. 5. A simple equivalent circuit consisting of an inductor (L), a resistor (R_0), and two RQ elements were employed to fit the impedance data. The left intercept with the impedance arc on the Z' (real) axis at high frequencies corresponds to the ohmic resistance, R_b, and the right intercept on the Z' axis indicates total resistance, R_{tot}. The polarization resistance, R_p, is the overall size of the arcs ($R_{tot} - R_b$). The temperature dependence of R_p is illustrated in Fig. 6. In the BSCoF and BSCuF samples, the polarization resistance values decreased remarkably with increasing Co and Cu content. The results are consistent with the concentration of oxide ion vacancies and electrical conductivities, as shown in Figs. 2 and 4, respectively. In comparison, between BSCoF, BSCuF, and LSCF, almost all of the BSCoF and BSCuF compositions yielded better electrochemical performance than the LSCF compositions, which had significantly higher electrical conductivities than the BSCoF and BSCuF in all atmospheres, except for the BSCuF80 composition that possessed a relatively large polarization resistance. This result implies that the quantity of oxide ion vacancies is more influential in electrochemical performance than the electrical conductivity.

Typical SEM micrographs of the cathodes on the GDC electrolyte after testing the single cell at 800 °C are shown in Fig. 7. The morphological images indicate that good adhesion is maintained between the layers, and the thickness of the cathode layer is about 20 μm. The LSCF layer displays a relatively fine grain size compared to others, although it was prepared using the same process to synthesize the powder and fabricate the single cells.

Variations in the *I–V* curve, power density, and cathode over-potential of the samples, which were constructed with the cathodes/GDC/Ni-YSZ configuration, are illustrated in Fig. 8. The electrochemical performance of the SOFCs was measured using humidified H_2 (~3 vol% H_2O) as a fuel and air as an oxidant, respectively, at 800 °C. The power density of the SOFCs increased and the over-potential of the cathodes decreased with increasing Co and Cu content, which agrees well with the impedance spectra data in Fig. 5. Since the oxygen reduction reaction is a complex catalytic reaction, the oxygen ion mobility, the surface exchange during the adsorption and dissociation of the oxygen molecule, and the electronic conductivity of the cathodes are all important factors for optimizing the electrochemical performance. As shown in Figs. 2 and 4, the concentration of the oxide ion vacancies and electrical conductivities increases with an increase in Co and Cu content. Generally, the oxygen

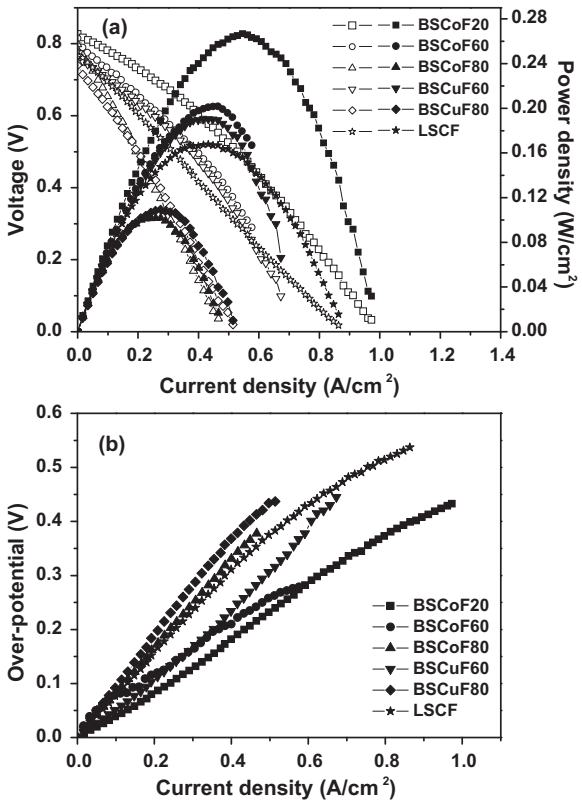

Fig. 8. Comparison of (a) the *I–V* curves (open symbols) and power densities (closed symbols) and (b) cathode over-potentials with various cathodes at 800 °C.

permeability is influenced by both oxide ion mobility and oxide ion vacancy concentration [36]. Likewise, the surface oxygen exchange coefficient is directly proportional to the mobile fraction of the oxide ion vacancies [37]. For these reasons, the addition of Co and Cu drives an increase in the electrochemical performance of BSCoF and BSCuF. The BSCoF60 and BSCuF60 compositions preformed slightly better while the BSCoF20 composition had a much better electrochemical performance than LSCF.

Since the impedance spectra under open circuit conditions can reflect the performances of the SOFCs, the results of the impedance spectra in Fig. 9 are consistent with those of the single cell test. The high frequency resistance is associated with charge transfer processes and the low frequency arc is attributed to the adsorption reaction and oxygen diffusion [8,38–40]. Consequently, the cathode impedance data in Fig. 9 indicate that the charge transfer processes influence BSCoF, and the diffusion processes affect BSCuF and LSCF as a rate-determining step. It should be noted that the R_p of the BSCoF cathode is much smaller than that of the whole single cell, while the R_p of the BSCuF and LSCF cathode are almost same. Thus, if the cells with the BSCoF cathode are optimized, the electrochemical performance could be improved further.

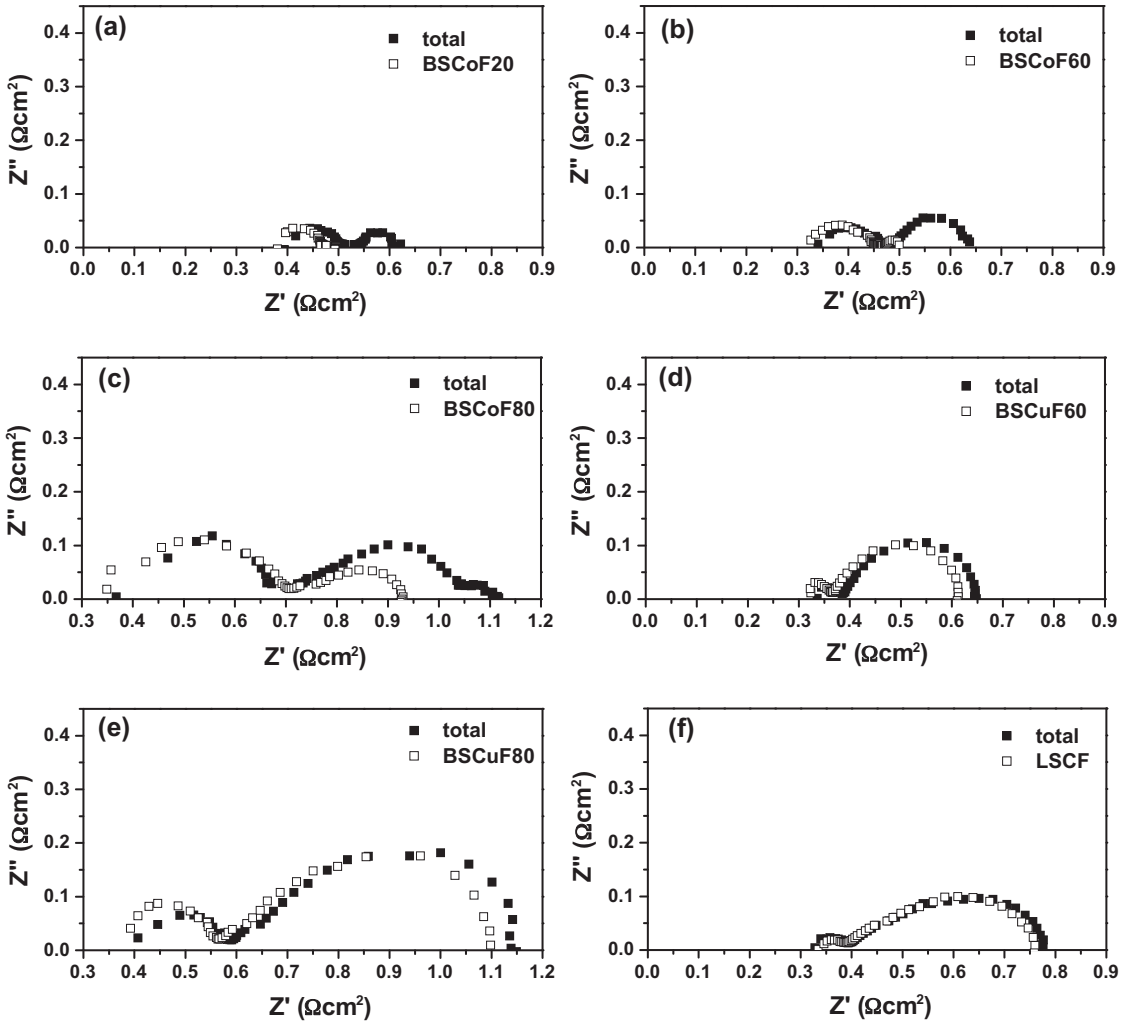

Fig. 9. Impedance spectra of the cathodes (open symbols) and the single cells (closed symbols) with the cathodes/GDC/Ni-YSZ configuration, measured under open-circuit conditions at 800 °C: (a) BSCoF20, (b) BSCoF60, (c) BSCoF80, (d) BSCuF60, (e) BSCuF80, and (f) LSCF.

4. Conclusions

The mixed conducting $Ba_{0.5}Sr_{0.5}Co_{1-x}Fe_xO_{3-\delta}$ ($x = 0.2$, 0.6 and 0.8) and $Ba_{0.5}Sr_{0.5}Cu_{1-x}Fe_xO_{3-\delta}$ ($x = 0.6$ and 0.8) oxide cathodes were synthesized by a citrate–EDTA complexing method. With increasing Co and Cu content, the polarization resistance values decreased dramatically due to an increase in the electrical conductivities and oxide ion vacancy concentrations, which are directly proportional to the surface oxygen exchange kinetics, while the TEC increased. Although the BSCoF and BSCuF samples had much lower electrical conductivities and a higher TEC than the LSCF sample, the majority of the BSCoF and BSCuF samples exhibited better power densities and lower cathode over-potentials than the LSCF sample in the single cell performance test. The maximum power density of BSCoF80, BSCoF60, BSCuF60, and LSCF at 800 °C was 266, 202, 190, and 167 mW/cm^2, respectively. It should be noted that the polarization resistances of the BSCoF cathodes were significantly lower than those of the whole single cell, while the polarization resistances of the BSCuF and LSCF cathodes were nearly identical to those of the whole single cells. Thus, using BSCoF cathode materials while fully optimizing the other relevant components will likely improve the electrochemical performance of the cathode.

Acknowledgments

This research was supported by the Basic Science Research Program through the National Research Foundation of Korea (NRF) funded by the Ministry of Education, Science and Technology (grant number: 2010-0009130). This work was also supported by the Human Resources Development of the Korea Institute of Energy Technology Evaluation and Planning (KETEP) grant funded by the Korea Government Ministry of Knowledge Economy (No. 20114030200060).

References

[1] R.A. De Souza, J.A. Kilner, Oxygen transport in $La_{1-x}Sr_xMn_{1-y}Co_yO_{3\pm\delta}$ perovskites. Part I. Oxygen tracer diffusion, Solid State Ionics 106 (1998) 175–187.

[2] S.P. Jiang, Issues on development of (La,Sr)MnO_3 cathode for solid oxide fuel cells, J. Power Sources 124 (2003) 390–402.

[3] L.W. Tai, M.M. Nasrallah, H.U. Anderson, D.M. Sparlin, S.R. Sehlin, Structure and electrical properties of $La_{1-x}Sr_xCo_{1-y}Fe_yO_3$. Part 1. The system $La_{0.8}Sr_{0.2}Co_{1-y}Fe_yO_3$, Solid State Ionics 76 (1995) 259–271.

[4] H. Ullmann, N. Trofimenko, F. Tietz, D. Stover, A. Ahmad- Khanlou, Correlation between thermal expansion and oxide ion transport in mixed conducting perovskite-type oxides for SOFC cathodes, Solid State Ionics 138 (2000) 79–90.

[5] S.P. Jiang, A comparison of O_2 reduction reactions on porous (La,Sr)MnO_3 and (La,Sr)(Co,Fe)O_3 electrodes, Solid State Ionics 146 (2002) 1–22.

[6] H. Zhao, W. Shen, Z. Zhu, X. Li, Z. Wang, Preparation and properties of $Ba_xSr_{1-x}CoyFe_{1-y}O_{3-\delta}$ cathode material for intermediate temperature solid oxide fuel cells, J. Power Sources 182 (2008) 503–509.

[7] Z. Chen, R. Ran, W. Zhou, Z. Shao, S. Liu, Assessment of $Ba_{0.5}Sr_{0.5}Co_{1-y}Fe_yO_{3-\delta}$ ($y = 0.0$–1.0) for prospective application as cathode for IT-SOFCs or oxygen permeating membrane, Electrochim. Acta 52 (2007) 7343–7351.

[8] W. Zhou, R. Ran, Z. Shao, W. Jin, N. Xu, Evaluation of A-site cation-deficient $(Ba_{0.5}Sr_{0.5})_{1-x}Co_{0.8}Fe_{0.2}O_{3-\delta}$ ($x > 0$) perovskite as a solid-oxide fuel cell cathode, J. Power Sources 182 (2008) 24–31.

[9] G.C. Kostogloudis, C. Ftikos, Properties of A-site-deficient $La_{0.6}Sr_{0.4}Co_{0.2}Fe_{0.8}O_{3-\delta}$-based perovskite oxides, Solid State Ionics 126 (1999) 143–151.

[10] V. Dusastre, J.A. Kilner, Optimisation of composite cathodes for intermediate temperature SOFC applications, Solid State Ionics 126 (1999) 163–174.

[11] P. Zeng, R. Ran, Z. Chen, H. Gu, Z. Shao, J.C. Diniz da Costa, S. Liu, Significant effects of sintering temperature on the performance of $La_{0.6}Sr_{0.4}Co_{0.2}Fe_{0.8}O_{3-\delta}$ oxygen selective membranes, J. Membr. Sci. 302 (2007) 171–179.

[12] A. Mai, V.A.C. Haanappel, S. Uhlenbruck, F. Tietz, D. Stover, Ferrite-based perovskites as cathode materials for anode-supported solid oxide fuel cells. Part I. Variation of composition, Solid State Ionics 176 (2005) 1341–1350.

[13] W.H. Kim, H.S. Song, J.W. Moon, H.W. Lee, Intermediate temperature solid oxide fuel cell using (La,Sr)(Co,Fe)O_3-based cathodes, Solid State Ionics 177 (2006) 3211–3216.

[14] Z. Shao, S.M. Haile, A high-performance cathode for the next generation of solid-oxide fuel cells, Nature 431 (2004) 170–173.

[15] W. Zhou, Z. Shao, R. Ran, Z. Chen, P. Zeng, H. Gu, W. Jin, N. Xu, High performance electrode for electrochemical oxygen generator cell based on solid electrolyte ion transport membrane, Electrochim. Acta 52 (2007) 6297–6303.

[16] W. Zhou, R. Ran, Z.P. Shao, H.X. Gu, W.Q. Jin, N.P. Xu, Significant impact of nitric acid treatment on the cathode performance of $Ba_{0.5}Sr_{0.5}Co_{0.8}Fe_{0.2}O_{3-\delta}$ perovskite oxide via combined EDTA–citric complexing process, J. Power Sources 174 (2007) 237–245.

[17] S. Li, Z. Lü, X. Huang, W. Su, Thermal, electrical, and electrochemical properties of Nd-doped $Ba_{0.5}Sr_{0.5}$ $Co_{0.8}Fe_{0.2}O_{3-\delta}$ as a cathode material for SOFC, Solid State Ionics 178 (2008) 1853–1858.

[18] B. Wei, Z. Lü, S. Li, Y. Liu, K. Liu, W. Su, Thermal and electrical properties of new cathode material $Ba_{0.5}Sr_{0.5}Co_{0.8}Fe_{0.2}O_{3-\delta}$ for solid oxide fuel cells, Electrochem. Solid-State Lett. 8 (2005) A428–A431.

[19] S. Li, Z. Lü, X. Huang, B. Wei, W. Su, Electrical and thermal properties of $(Ba_{0.5}Sr_{0.5})_{1-x}Sm_xCo_{0.8}Fe_{0.2}O_{3-\delta}$ perovskite oxides, Solid State Ionics 178 (2007) 417–422.

[20] S. Lee, Y. Lim, E.A. Lee, H.J. Hwang, J.W. Moon, $Ba_{0.5}Sr_{0.5}Co_{0.8}Fe_{0.2}O_{3-\delta}$ (BSCF) and $La_{0.6}Ba_{0.4}Co_{0.2}Fe_{0.8}O_{3-\delta}$ (LBCF) cathodes prepared by combined citrate–EDTA method for IT-SOFCs, J. Power Sources 157 (2006) 848–854.

[21] M. Chen, B.H. Kim, Q. Xu, B.K. Ahn, W.J. Kang, D.P. Huang, Synthesis and electrical properties of $Ce_{0.8}Sm_{0.2}O_{1.9}$ ceramics for IT-SOFC electrolytes by urea-combustion technique, Ceram. Int. 35 (2009) 1335–1343.

[22] J. Jung, S.T. Misture, D.D. Edwards, Oxygen stoichiometry, electrical conductivity, and thermopower measurements of BSCF ($Ba_{0.5}Sr_{0.5}Co_xFe_{1-x}O_{3-\delta}$, $0 \le x \le 0.8$) in air, Solid State Ionics 181 (2010) 1287–1293.

[23] B. Liu, Y. Zhang, L. Tang, X-ray photoelectron spectroscopic studies of $Ba_{0.5}Sr_{0.5}Co_{0.8}Fe_{0.2}O_{3-\delta}$ cathode for solid oxide fuel cells, Int. J. Hydrogen Energy 34 (2009) 435–439.

[24] M.S. Kim, J.B. Yang, P.E. Parris, Q. Cai, X.D. Zhou, W.J. James, W.B. Yelon, D. Buddhikot, S.K. Malik, The effect of Cu-doping on the magnetic and transport properties of $La_{0.7}Sr_{0.3}MnO_3$, J. Appl. Phys. 97 (2005) 10H714.

[25] J. Wackerl, T. Koppitz, D.H. Peck, S.K. Woo, T. Markus, Correlation of thermal properties and electrical conductivity of $La_{0.7}Sr_{0.3}Cu_{0.2}Fe_{0.8}O_{3-\delta}$ material for solid oxide fuel cells, J. Appl. Electrochem. 39 (2009) 1243–1249.

[26] A. Mineshige, J. Izutsu, M. Nakamura, K. Nigaki, J. Abe, M. Kobune, S. Fujii, T. Yazawa, Introduction of A-site deficiency into $La_{0.6}Sr_{0.4}Co_{0.2}Fe_{0.8}O_{3-\delta}$ and its effect on structure and conductivity, Solid State Ionics 176 (2005) 1145–1149.

[27] Y.H. Lim, J. Lee, J.S. Yoon, C.E. Kim, H.J. Hwang, Electrochemical performance of $Ba_{0.5}Sr_{0.5}Co_xFe_{1-x}O_{3-\delta}$ ($x = 0.$ 2–0.8) cathode on a ScSZ electrolyte for intermediate temperature SOFCs, J. Power Sources 171 (2007) 79–85.

[28] J. Ovenstone, J.I. Jung, J.S. White, D.D. Edwards, S.T. Misture, Phase stability of BSCF in low oxygen partial pressures, J. Solid State Chem. 181 (2008) 576–586.

[29] P.M. Raccah, J.B. Goodenough, First-order localized-electron ⇄ collective-electron transition in $LaCoO_3$, Phys. Rev. 155 (1967) 932–943.

[30] V.G. Bhide, D.S. Rajoria, Y.S. Reddy, G. Rama Rao, G.V. Subba Rao, C.N. Rao, Localized-to-itinerant electron transitions in rare-earth cobaltates, Phys. Rev. Lett. 28 (1972) 1133–1136.

[31] A.R. Ruffa, Thermal expansion in insulating materials, J. Mater. Sci. 15 (1980) 2258–2267.

[32] M. Mori, N.M. Sammes, Sintering and thermal expansion characterization of Al-doped and Co-doped lanthanum strontium chromites synthesized by the Pechini method, Solid State Ionics 146 (2002) 301–312.

[33] V. Ramaswamy, P. Awati, A.K. Tyagi, Lattice thermal expansion of $LaCo_{1-x}Cu_xO_3$, J. Alloys Compd. 364 (2004) 180–185.

[34] L.W. Tai, M.M. Nasrallah, H.U. Anderson, D.M. Sparlin, S.R. Sehlin, Structure and electrical properties of $La_{1-x}Sr_xCo_{1-y}Fe_yO_3$. Part 2. The system $La_{1-x}Sr_xCo_{0.2}Fe_{0.8}O_3$, Solid State Ionics 76 (1995) 273–283.

[35] K.T. Lee, A. Manthiram, $LaSr_3Fe_{3-y}Co_yO_{10-\delta}$ ($0 \le y \le 1.5$) intergrowth oxide cathodes for intermediate temperature solid oxide fuel cells, Chem. Mater. 18 (2006) 1621–1626.

[36] A. Manthiram, F. Prado, T. Armstrong, Oxygen separation membranes based on intergrowth structures, Solid State Ionics 152–153 (2002) 647–655.

[37] H. Bouwmeester, M. Otter, B. Boukamp, Oxygen transport in $La_{0.6}Sr_{0.4}Co_{1-y}Fe_yO_{3-\delta}$, J. Solid-State Electrochem. 8 (2004) 599–605.

[38] F.M. Figueiredo, J.R. Frade, F.M.B. Marques, Performance of composite $LaCoO_3$–$La_2(Zr,Y)_2O_7$ cathodes, Solid State Ionics 135 (2000) 463–467.

[39] X.J. Chen, K.A. Khor, S.H. Chan, Identification of O_2 reduction processes at yttria stabilized zirconia-doped lanthanum manganite interface, J. Power Sources 123 (2003) 17–25.

[40] J. Chen, F. Liang, B. Chi, J. Pu, S.P. Jiang, L. Jian, Palladium and ceria infiltrated $La_{0.8}Sr_{0.2}Co_{0.5}Fe_{0.5}O_{3-\delta}$ cathodes of solid oxide fuel cells, J. Power Sources 194 (2009) 275–280.